PROCEEDINGS, 49th Workshop on Geothermal Reservoir Engineering
Stanford University, Stanford, California, February 12-14, 2024
SGP-TR-227

A Novel Workflow for Coupled Simulation of Hydraulic Stimulation with Simultaneous Injection of Proppant

Robert Egert[1], Chunfang Meng[2,3], Aimé Fournier[3] and Wencheng Jin[1,*]

[1]Energy and Environment Science and Technology Directorate, Idaho National Laboratory, USA

[2]Eden Geopower, Somerville, Massachusetts, USA

[3]MIT Earth Resources Laboratory, Cambridge, Massachusetts, USA

robert.egert@inl.gov, wencheng.jin@inl.gov

Keywords: Proppant transport, hydraulic fracturing, radial fracture, numerical modeling

ABSTRACT

Stimulating reservoirs through the creation of hydraulically conductive fractures is a key step for enabling geothermal energy utilization and conducting in-situ mining in hard rock formations. The effectiveness of hydraulic fracturing is intricately tied to both the fracturing scheme employed and the deposition and accumulation of proppant within induced fractures. Geomechanical parameters of the host rock play a critical role in influencing fracture propagation, while the transport and settling of proppant, affected by the rheology of the fracturing fluid, concentration, and the geometry of the fractures, determines the residual aperture distribution after shut-in. This study introduces ELK (ELectrical fracKing), an innovative computational application designed for the coupled numerical simulation of hydraulic fracturing and the injection and circulation of proppant-fluid mixtures within a fractured host rock. ELK serves as a valuable tool for designing and optimizing subsequent reservoir simulations and utilization strategies. This application is based on the open-source MOOSE framework and has been enriched with a set of equations to govern the circulation of proppant-laden slurries. It accounts for both the fluid and proppant components of the mixture, as well as particle-driven processes like gravitational settling, particle-particle interactions, and concentration-dependent density/viscosity. A particular challenge is the mutual coupling with fracture mechanical processes in a propagating fracture, either included as analytical equations or simulated using fracture mechanics tools like the MOOSE-based application KitFox. Aperture and fluid pressure on one side and slurry density and viscosity changes on the other side interact and affect each other. Basic understanding of these is essential for the success of the stimulation. The simple coupling of both numerical codes shows promising results regarding the simultaneous modeling of both physical processes and will be developed further to predict field-scale hydraulic fracturing with high accuracy.

1. INTRODUCTION

Hydraulic fracturing is a methodology employed to create or enhance fractures and fracture networks in low-permeable formations, thereby increasing the permeability of the overall reservoir. This technique finds application in diverse geoscientific contexts, including enhanced geothermal systems (EGS) (Jia et al. 2022), unconventional reservoirs (Aslannezhad et al. 2021), or in-situ mining (Parker and Jupe 1997). The multistage process of hydraulic fracturing involves rock deformation induced by fluid pressurization and cracking, fluid flow within the fracture, and fracture propagation (Chen et al. 2021). A substantial volume of water is injected through a wellbore into the reservoir, initiating, enlarging, and propagating fractures. However, upon release of fluid pressure, in-situ stress would cause fracture closure, and the previously created pathways to be blocked again (Barboza et al. 2021). To counteract this, proppants - like small graphite or sand particles - are added to the fracturing fluid, the so-called slurry. The retained proppant particles settle out and maintain the fracture aperture, while the fracturing fluid propagates into the surrounding matrix or is extracted from the wellbore (Wang 2020). Indeed, the proppant distribution is a crucial factor for the success of hydraulic stimulation (Barboza et al. 2021). Achieving an optimal distribution of fractures and particles therein requires careful consideration of the injection strategy and the properties of both the rock and the slurry (Huang et al. 2022). Extensive experimental studies on proppant dispersion and settling, conducted at laboratory and field scales, provide a foundation for developing empirical correlations (Isah et al. 2021, Yao et al. 2022).

Hydraulic stimulation at the field scale is significantly impacted by the often-unknown characteristics of the subsurface (Zhang et al. 2022). Despite this uncertainty, numerical simulations play a crucial role in identifying, quantifying, and predicting the physical processes involved in the hydraulic stimulation process. In principle, the processes can be split into two main physical processes. On the one hand, any kind of fluid flow in fractured rock is simulated via the lubrication theory, including fluid flow velocity, fracture width and pressure gradient (Egert et al. 2021). On the other hand, solid rock deformation can be modeled assuming the theory of linear (fracture) elasticity establishing the relationship between fracture width and fluid pressure (Adachi et al. 2007). The inclusion of proppant transport during stimulation introduces an additional layer of complexity. This aspect necessitates treating fluid flow as a multiphase and/or multi-component flow problem involving two interpenetrating media (Barboza et al. 2021). For computational efficiency, Eulerian-Eulerian numerical schemes are frequently employed, treating both the fracturing fluid and proppant as continua governed by mass conservation principles (Shiozawa and McClure 2016). The simulation of slurry transport is often conducted as a mixture flow, with a concentration-dependent fluid rheology (Kumar et al. 2019, Egert et al. 2023). Physical processes like particle-particle interactions and the resulting relative motion rely on empirically derived correlations (Huang et al. 2022).

Predicting hydraulic stimulation has a longstanding history, evolving from initial mathematical descriptions to contemporary fully-coupled numerical simulations. The progress in this area reflects the continuous advancements in understanding the complex processes involved in hydraulic stimulation. Seminal works were done by Perkins and Kern (1961) (PK model), Geertsma and De Klerk (1969) (KGD model) and Nordgren (1972) (PKN model), describing fracture width and height in relationship to the rock geomechanical properties, fluid viscosity and injection rate. The interplay between viscous flow, fracture surface creation, and fluid storage in fractures or leak-off in the matrix exerts competing effects that significantly influence fracture propagation. The behavior of propagation can be grouped into four distinct regimes, determined by the dominant effects and problem parameters (viscosity/storage domination, toughness/leak-off domination) as outlined by Detournay (2016). The advantage of these regimes is that their representative members can be solved analytically for the models described (PKN, KGD and radial fracture) and therefore serve as validation for numerical codes (Dontsov 2016). Numerous computational approaches have been studied to replicate the simplified single fracture solutions and to simulate more intricate hydraulic stimulation treatments. These numerical approaches can be roughly divided into continuum-based and discontinuous methods and differ as to whether the crack path is known a priori or not (Chen et al. 2021). The most popular methods are the finite element method (FEM) and specializations like extended finite element (XFEM) (Jin and Arson 2019), phase field modeling (PFM) (Costa et al. 2023), cohesive zone modeling (CZM) (Liu et al. 2023), or split node (Meng et al. 2023). In contrast to the well-explored research of hydraulic fracturing simulation, the coupled simulation that involves simultaneous transport of proppant is relatively limited and numerically challenging. Wang (2020) developed a fully-coupled numerical code to capture hydraulic stimulation with proppant including proppant bank formation. Hosseini and Khoei (2020) simulated proppant transport and tip screen-out in hydraulic fracturing with XFEM. Zeng et al. (2019) coupled proppant transport to the analytical solution of the classical PKN model.

In this study, our focus is on the coupled simulation of proppant transport within a propagating fracture, and we outline the steps taken toward achieving this objective. Initially, we calibrate the proppant transport workflow by comparing it against experimental results. The experiment involves injecting a slurry composed of water and high-density proppant into a 2D vertical, parallel-walled fracture with a constant aperture. Moving to the next step, we simulate the hydraulic fracturing of a radial (penny-shaped) fracture using CZM. Finally, we present preliminary work on the coupled simulation of proppant transport within a propagating fracture. Collectively, these steps contribute to advancing our understanding of the complex interplay between hydraulic fracturing and proppant movement.

2. METHODS

The numerical modeling of proppant propagation is carried out with the finite element (FE) application ELK (ELectrical fracKing) (Egert et al. 2023). This code is built on the open-source MOOSE (Multiphysics Object-Oriented Simulation Environment) framework (Lindsay et al. 2022) and leverages its PorousFlow module (Wilkins et al. 2021) for a fully coupled solution of thermo-hydraulic processes in porous and fractured media. The governing equations were extended to consider concentration-dependent fluid rheology. CZM is conducted with the MOOSE-based app KitFox (Liu et al. 2023), which implements a modified incomplete interior penalty Galerkin (IIPG) formulation as discontinuous Galerkin (DG) kernels, and a linear extrinsic cohesive law into MOOSE. Coupling between both codes is realized using the MOOSE MultiApp interface (Gaston et al. 2015). Both ELK and KitFox provide flexibility for multidimensional analysis and solution of physical processes, allowing consideration of 3D lithologic units, as well as lower dimensions such as 2D fractures and 1D wells.

2.1 Slurry and proppant flow

The fundamental governing equations solved in ELK are based on mass and momentum balances for both the fracturing fluid and the proppant particles, treated as a single-phase mixture and solved as continua of interpenetration. In this approach, a volume cell can be simultaneously occupied by a mixture of both components. The gravitational settling out of the slurry and bedding formation is controlled by the contrast between the fracturing fluid and proppant. In addition, a concentration-dependent fluid rheology is considered in the model through changes in density and viscosity. The equations used, their derivations and empirical formulations are presented in detail in Egert et al. (2023).

The following mass balance is solved for slurry flow:

$$\frac{\partial}{\partial t}(\rho_m) + \nabla \cdot (\rho_m v_m) = 0, \tag{1}$$

where ρ_m is the slurry (mixture) density, v_m is the Darcy velocity vector of the slurry

$$v_m = -\frac{k_f}{\mu_m}(\nabla p - \rho_m g), \tag{2}$$

p is the slurry pressure, μ_m is the viscosity of the slurry, and g is the gravity vector. The fracture permeability k_f is dependent on the fracture aperture a and established coupling to the geomechanics application. The permeability is calculated assuming the fracture walls could be represented as two parallel plates and assuming the local cubic law (Egert et al. 2021):

$$k_f = \frac{a^2}{12}. \tag{3}$$

The mass conservation for the proppant in a lower-dimensional fracture can be obtained using

$$\frac{\partial}{\partial t}(c\ a)\ +\ \nabla\cdot(c\ a\ v_p)\ =\ 0, \tag{4}$$

where $c = (\rho_m - \rho_f)/(\rho_p\ -\ \rho_f)$ and v_p denote the proppant fraction and velocity, respectively. The proppant particle velocity v_p is related to the carrying fluid velocity by the slip velocity v_{slip}:

$$v_p\ =\ v_m\ +\ (1-c)\frac{\rho_f}{\rho_m}v_{slip}. \tag{5}$$

The slip velocity v_{slip} encompasses various effects that cause the particle velocity to deviate from the slurry velocity. These effects include, but are not limited to, gravitational particle settling, collisional effects, fluid-particle drag forces, and turbulent mixing effects. Further details, including empirical equations for particle-particle interactions, turbulent settling conditions and different concentration-dependent viscosity laws, can be found e.g., in Egert et al. (2023).

2.2 Hydraulic fracturing

KitFox extends the RCZM module presented in Liu et al. (2023) for solid-material crack propagation to model hydraulic fracturing in porous media. Hydraulic fracturing is governed by three field equations coupling solid mechanics, fluid flow in bulk porous media and fluid flow in the narrow fracture as follows (Liu et al. 2024):

$$\nabla\cdot\sigma + f = 0 \qquad on \quad \Omega\backslash\Omega^a, \tag{6}$$

$$\alpha\dot{\varepsilon}_v + \frac{1}{M}\dot{p} + \nabla\cdot q = s_q \quad on \quad \Omega\backslash\Omega^a, \tag{7}$$

$$\dot{a}_a + \nabla\cdot q_a = s_a \qquad on \quad S^a, \tag{8}$$

where Ω is the full domain, Ω^a is the set of all interior cracked sub-domains, S^a is the intermediate surface, σ is the Cauchy stress tensor, q denotes the porous-medium flux, and q_a is the flux within the fracture aperture. The injection rate into the matrix and fracture are denoted by s_q and s_a, respectively. $\dot{\varepsilon}_v$ is the volumetric strain rate of the solid skeleton. The superscript a indicates that equation 8 is restricted to the aperture of the fracture. Further details on the numerical implementation of linear elasticity in the solid phase, IIPG, RCZM, as well as crack initiation and propagation, is presented and discussed in Liu et al. (2023). Darcy flow in the porous matrix and poroelasticity are described in Wilkins et al. (2021).

2.3 Coupling approach

The coupling approach employed in this study relies on the MultiApp feature introduced into the MOOSE framework (Gaston et al. 2015). This feature facilitates multidimensional coupling in either a full or loose manner, providing flexibility and efficiency in integrating different components of the simulation. Different kinds of physics can be solved, uncoupled, in time and space, and then exchanged via spatial properties, variables, or shape functions. A main app plays a key role in defining the exchange between itself and the different sub-apps, contributing to the overall coordination, convergence criteria and synchronization of the coupled simulation. A sub-app can be executed at any time during the main app solve e.g., loosely after each time step of the main app, or fully coupled through fixed-point iterations during the solve.

In this study, a loose coupling strategy is implemented, where the main application (ELK) is solved after the sub-application KitFox completes its calculations. Time steps are synchronized between both applications, ensuring that each time step is addressed by both. If an application encounters an issue during the solution process, the particular time step is reduced, allowing the failed app to continue solving until it catches up. The mesh is shared between both apps. Nodal and elemental variables are used to transfer the different material properties between the apps. The sub-app solves for pressure and aperture and transfers these to the main app. While pressure is defined across the entire domain, the aperture is limited to the fracture plane, often described as an interface or lower-dimensional block. The aperture information in the main app is utilized to derive the fracture permeability using the local cubic law (Witherspoon et al. 1980), and porosity is employed as a scaling parameter to quantify the lower-dimensional mass flow. ELK calculates the proppant transport (limited to the fracture plane) and updates concentration-dependent material parameters like fluid density and viscosity. These could be transferred back into the sub-app.

3. RESULTS

3.1 Multi-Inlet Proppant Injection

We compare the developed proppant transport code ELK against a slot experiment conducted by Chun et al. (2020) and the numerical benchmark in Huang et al. (2022). The experiment involved injecting slickwater into a single vertical fracture through three individual inlets, with the fracture constrained by Plexiglas to mimic an impermeable rock and allow visual observation. The dimensions of the fracture were 1.2 × 0.3 m^2, maintaining a constant fracture width of 7.62 mm. Three circular inlets, each 12.7 mm in diameter, were positioned on the right side of the fracture with a spacing of 76.2 mm between them. The premixed slurry was injected with a constant rate of 0.378 $l{\cdot}s^{-1}$ and a concentration of 0.07. An outlet in the upper left corner allowed fluid to escape. Pure water and sand were used as the carrying fluid and the proppant, respectively.

Table 1: Experimental setup after Chun et al. (2020).

Parameter	Unit	Value
Fracture width	m	0.00762
Fracture length	m	1.2192
Fracture height	m	0.3048
Inlet slurry rate	$m^3 \cdot s^{-1}$	0.000378
Proppant density	$kg \cdot m^{-3}$	2550
Proppant diameter	m	0.000415
Proppant inlet concentration	-	0.07
Proppant saturation concentration	-	0.62
Carrying fluid density	$kg \cdot m^{-3}$	1000
Carrying fluid dynamic viscosity	Pa·s	0.001
Outlet pressure	Pa	(atmosphere)

Figure 1 illustrates the results of our simulations against the experimental data, and further numerical results. The findings reveal that settling is the primary driving force for the movement of dense particles in the low-viscosity-carrying fluid (water). In the initial stage (t = 10 s), most particles settle in the first third of the entire fracture, forming a growing immobile proppant bed indicated by the dark red colors (and maximum saturation). Dark blue colors indicate that large portions of the fracture aren't affected by the proppant, and no proppant flows through the outlet. Towards the end of the experiment (t = 30 s), a dune forms near the inlets, clogging most of the fracture in the vertical direction. In proximity to the lower and middle inlets on the right side of the fracture, a zone characterized by high advection velocities and strong internal mixing emerges. This mixing zone could be reproduced, with sufficient precision. The challenges in reproducing the maximum height and propagating slope of the dune can be attributed to the characteristics of the finite element method, especially the necessity for upwinding to stabilize highly convective systems. While upwinding is crucial for ensuring numerical stability, it introduces overdiffusion in the system. This overdiffusion is a contributing factor to the observed discrepancy between the experimental observation of the fracture being mostly clogged and our simulation predicting a maximum dune height of 2/3 of the fracture height. This also results in increased maximum bedding length compared to the experimental results.

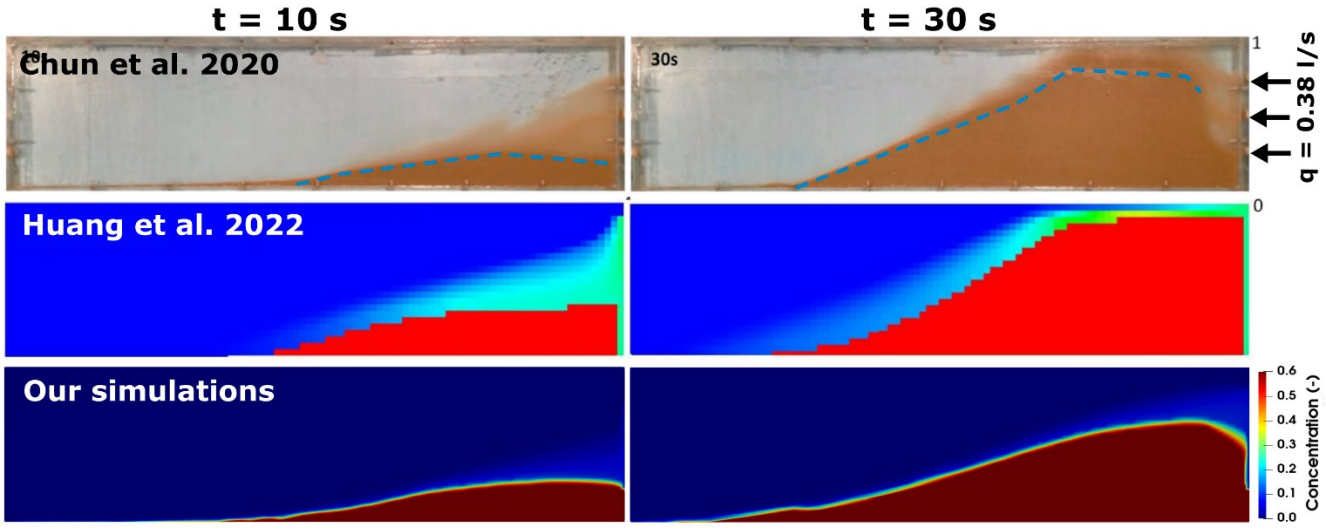

Figure 1: Comparison of our numerical results with the experimental results of Chun et al. (2020) and the simulations presented in Huang et al. (2022).

3.2 Radial hydraulic fracture model

The KitFox app has been successfully benchmarked against the commonly used KGD (plane strain) model (Liu et al. 2024). The KGD assumes that fracture width is independent of the fracture height (Adachi et al. 2007). Given the rectangular cross-sectional area and fixed size of this model, it is not suitable for later coupling with gravitational-induced particle settling in the context of this study. Therefore, the simulations are extended to a 3D penny-shaped or radial hydraulic fracturing model. This model assumes a borehole parallel to the minimum principal stress, and that the fracture extends vertically around a horizontal borehole. The governing equations used in this model are analogous to the KGD model, but with the plane strain assumption replaced by an axisymmetric assumption. This model considers a penny-shaped hydraulic fracture propagating within an infinite linear elastic medium subjected to confining stress. The fracture length and height (aperture) grow with time and continuous fluid injection (Chen et al. 2021). A sketch of the proposed setup is shown in Figure 2. The numerical results will be compared to the analytical solution of a toughness-storage dominated solution as presented in Dontsov (2016).

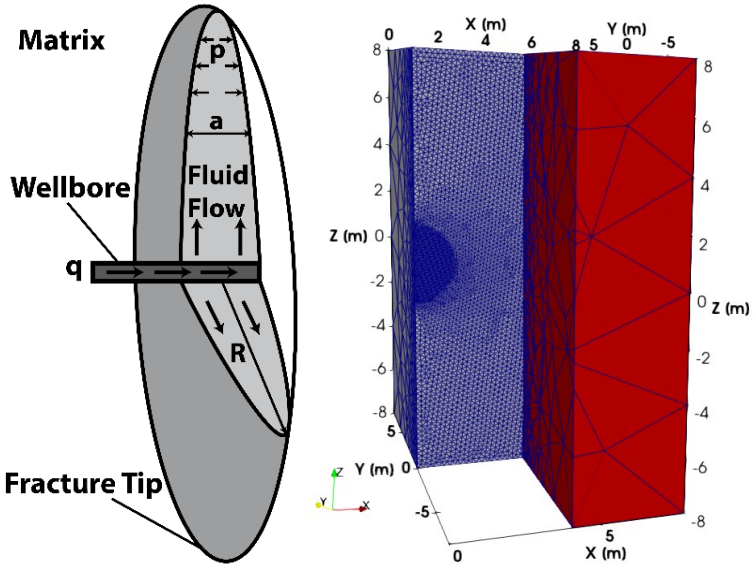

Figure 2: Left: Sketch of a penny-shaped hydraulic fracture model including fluid flow and growth in fracture length/width. Right: The mesh used for simulation. Shown are the different matrix blocks and the refinement along the fracture plane.

The model shown in Figure 2 (left) assumes a prescribed planar fracture surrounded by a 3D low-permeable matrix. For computational efficiency, the model is mirrored along the YZ-plane. It has dimensions of 8×14×8 cubic meters and consists of 25 659 nodes. Refinement is implemented along the fracture plane and near the proposed injection point. All boundaries are set to roller boundary conditions, enabling movement parallel to the boundary plane while fixing movement in the normal direction. Additionally, a Dirichlet boundary condition with a pressure of 0 Pa is applied at the right boundary of the model. A continuous injection of 1 $kg{\cdot}s^{-1}$ is applied as a point source at the origin of the coordinates. The interface between both matrix blocks is defined as a discontinuous Galerkin interface where both CZM and aperture fluid flow are solved. A notch with an initial fracture aperture ($a = 10^{-4}$ m) and permeability close to the injection point (radius = 0.05 m) is introduced to prevent singularity in the first timestep and enhance numerical convergence. A minimum aperture ($a = 10^{-7}$ m) is used for numerical stability. The simulation time is limited to 20 s. Further parametrization is shown in Table 2.

Table 2: Storage-Toughness dominated radial fracture simulation parameters.

Parameter	Unit	Value
Young's modulus	GPa	17
Poisson ratio	-	0.2
Biot coefficient	-	0.75
Biot modulus	MPa	68.7
Injection rate	$kg{\cdot}s^{-1}$	1
Matrix permeability	m^2	10^{-16}
Matrix porosity	-	0.2

Fluid density	$kg \cdot m^{-3}$	1000
Fluid dynamic viscosity	Pa·s	10^{-4}
Fluid bulk modulus	GPa	2
Fracture energy	Pa	120
Fracture failure strength	MPa	0.625
Fracture aperture	m	(local cubic law)

The results of the numerical modeling are shown in Figure 3 for the timesteps 10 s and 20 s. The fracture develops radially around the injection point. At the beginning of the injection, the borehole pressure reaches values exceeding 2 MPa, which gradually decreases to 0.6 MPa by the end of the simulation (t = 20 s). Due to the low host-rock permeability, just a small amount of pressure diffuses into the matrix. Initially, a strong pressure gradient develops within the fracture and towards the fracture tip, which diminishes towards the end of the simulation, resulting in a mostly homogeneous pressure field within the fracture (t = 20 s). The aperture field evolves over time, with the maximum aperture reaching 0.25 mm near the borehole by the end of the simulation. Along the fracture plane, the aperture gradually decreases towards the fracture tip. The horizontal stress is shown in Figure 4. High tensile stress around the fracture tip and compressive stress on the wake of the fracture are visible. The compressive horizontal stress on the wake of the fracture arises from the applied fluid pressure loading on the fractured walls.

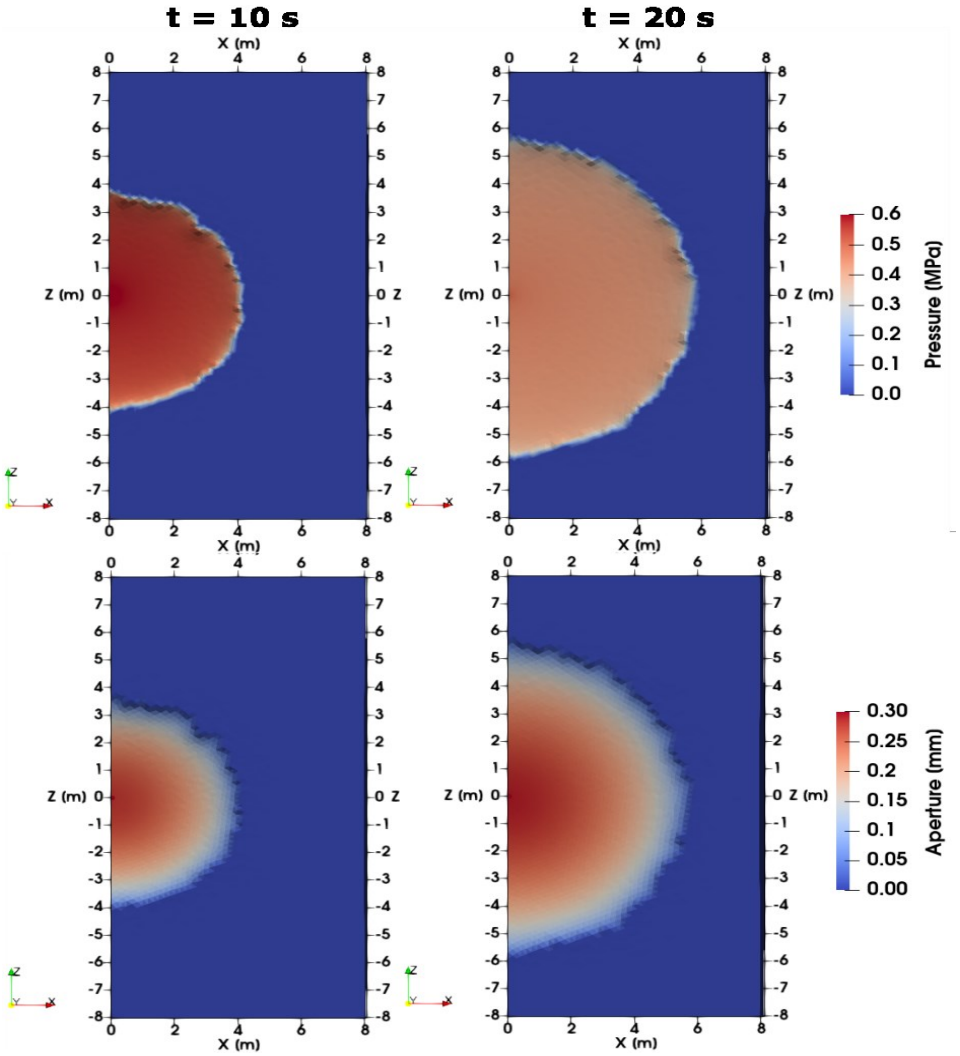

Figure 3: Results of the numerical simulation for pressure and aperture at the fracture plane for t = 10 s and t = 20 s.

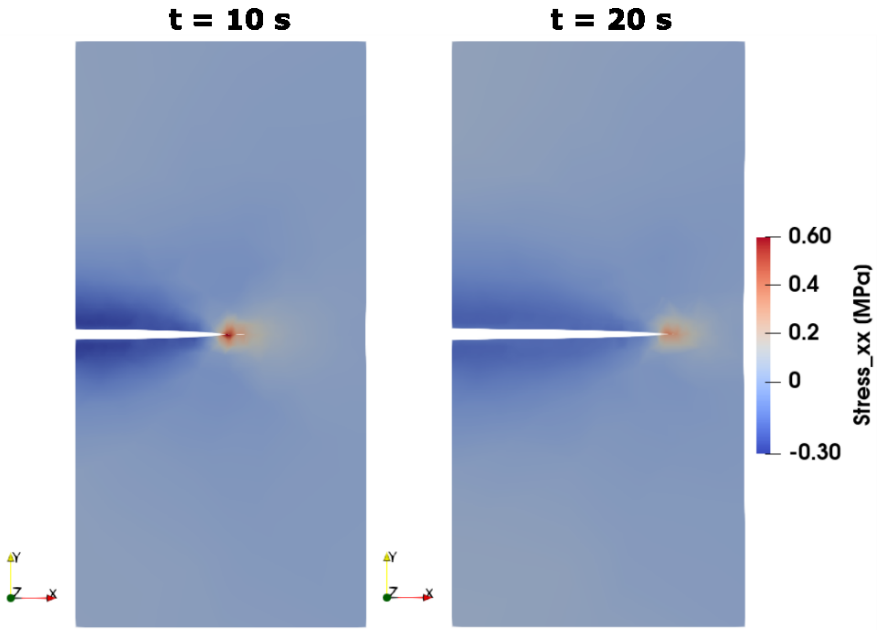

Figure 4: Cross-section through the propagating fracture at the center. Shown is the horizontal stress for $t = 10$ s and $t = 20$ s.

Figure 5 illustrates the characteristic properties of our simulation (red dots and line) compared to the analytical solution (blue line) presented in Dontsov (2016). At the borehole, fracture width and fluid pressure are compared. The results demonstrate a good agreement between our simulation and the analytical equation for toughness-storage dominated radial fractures. However, a slightly higher borehole fluid pressure is observed between 3 and 12 s, which results in a slight increase in aperture during these timesteps. The fracture radius matches perfectly with the predicted results. The non-smooth simulation results are attributed to the mesh size and the fact that fracture propagation occurs element-wise. Further mesh refinement would lead to higher precision.

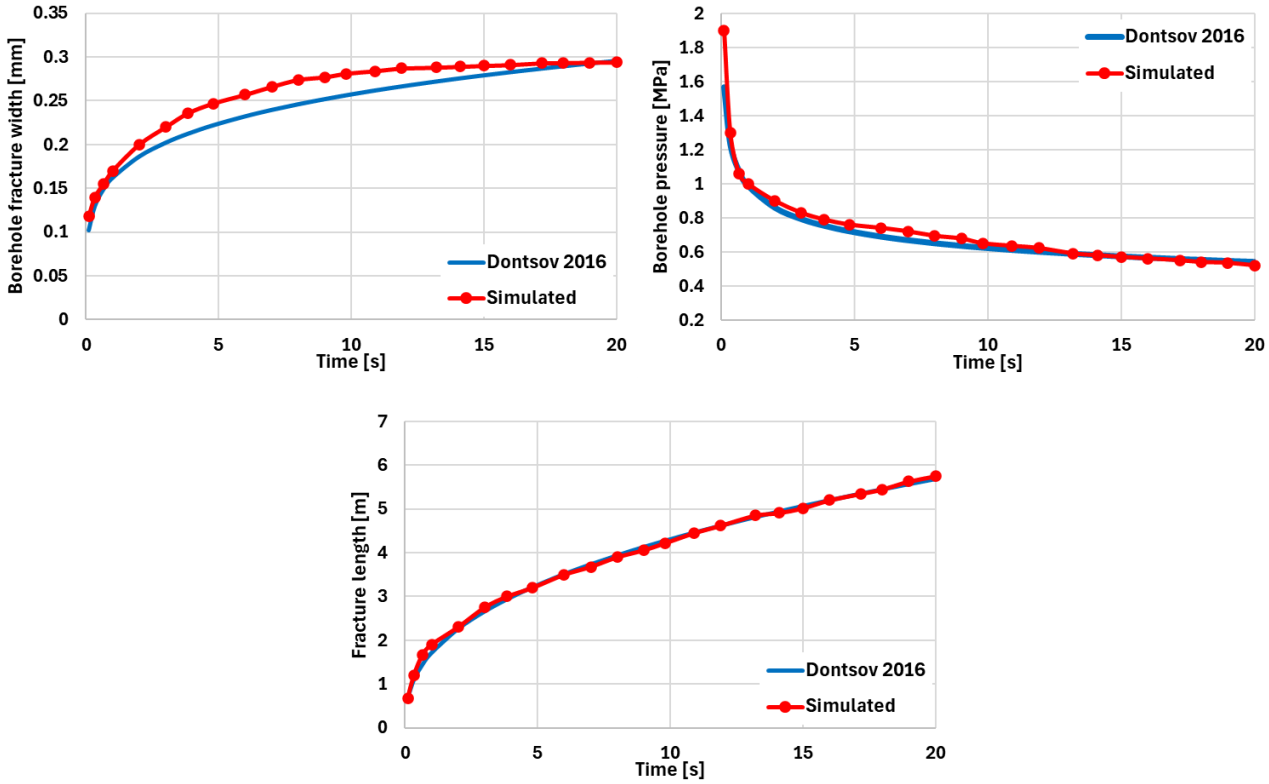

Figure 5: Comparison of the numerical model against the analytical solution presented in Dontsov (2016). Compared are the fluid pressure at the borehole, the fracture width at the borehole and the fracture length versus time during continuous injection.

3.3 Coupled simulation of proppant transport in a radial extending fracture

In the final model, we integrate the developed slurry and proppant transport code with the hydraulic fracturing code to accurately model the hydraulic fracturing process while injecting high-density slurry. A MultiApp workflow is developed to couple both applications, initially focusing on limited coupling and transfer of certain variables. In the workflow, both applications share the same mesh, with limited MOOSE-internal modifications in the representation of the 2D fracture plan as either discontinuous Galerkin interface (KitFox) or 2D lower-dimensional elements with aperture as scaling parameter (ELK). The KitFox application is solved first, and variables (like pressure and aperture) are transferred to the main ELK application. These variables are used as input for the nonlinear (pressure) and to calculate the aperture and permeability of the 2D fracture. The proppant transport is solved for the same timestep, and variables (like density and viscosity) could get transferred back into the sub-app to run the next timestep. The simulation depicted below is built upon the hydraulic fracturing model previously introduced in Section 3.2. The input for the sub-app uses the parametrization presented in Table 2. Instead of pure water (with 1 $l \cdot s^{-1}$), a slurry with a concentration of 0.1 is injected, and concentration-dependent density and viscosity changes are considered in the main application. The maximum concentration is 0.6, and the proppant density is assumed as 2500 $kg \cdot m^{-3}$. Due to the proppant particle size, proppant flow is limited to the fracture plane.

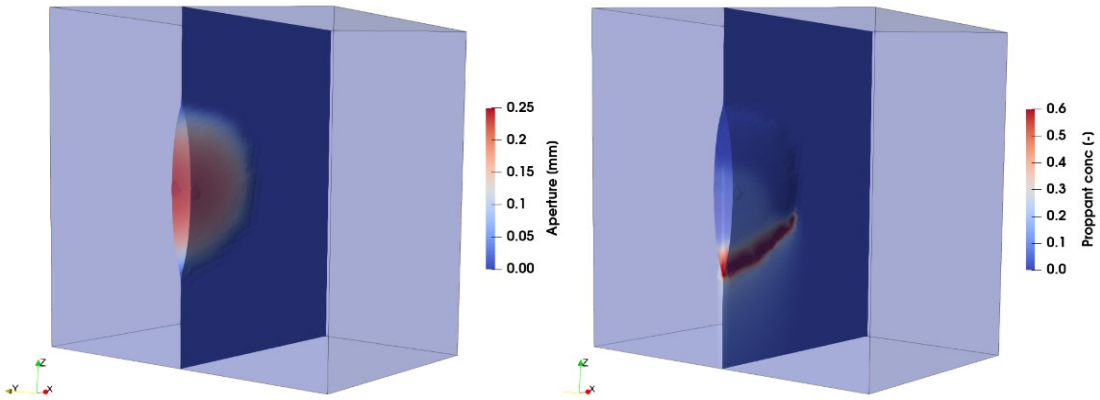

Figure 6: The 3D model at $t = 2.8$ s. Shown are the fracture aperture (left) and the proppant accumulating at the fracture bottom (right). Note: The visual displacement of both fracture surfaces is scaled by factor 1000.

Figure 6 shows exemplarily the 3D model, including the 3D matrix and the fracture. Aperture and proppant distribution are shown for $t = 2.8$ s. The preliminary results are consistent with the expected behavior. In the initial phase, a significant internal pressure gradient develops within the fracture void space and increases towards the propagating fracture tip (Figure 7). It is worth mentioning that the pressure gradient and the fluid lag at the fracture tip have limited effects on the transportation of proppant, as the proppant mainly remains in the open fracture void space. Thus, the internal pressure gradient along the already opened fracture is more influential for proppant transportation. During the early stages of the hydraulic fracturing process, the internal pressure gradient is most pronounced, resulting in a radial distribution of the proppant around the injection point. As fluid infiltrates the matrix around the fracture, proppant accumulates primarily in the smaller aperture regions near the fracture tip. With increasing simulation time and fracture length, the injection-related internal pressure gradient decreases, leading to a reduced slurry velocity. Interestingly, the increased density leads to a renewed increase in pressure with a higher amount of proppant in the fracture.

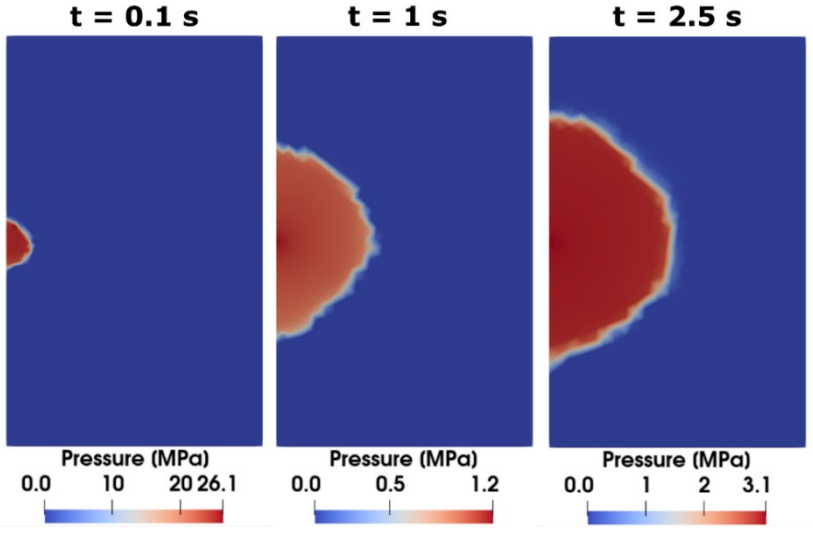

Figure 7: Pressure distribution along the fracture plan with increasing time.

Figure 8 illustrates the propagating fracture with increasing aperture and fracture length during continuous injection, along with the spatial proppant concentration and resulting slurry density. As stimulation time progresses, the initial radial proppant distribution is increasingly influenced by gravitational settling, leading to proppant settling at the bottom of the fracture. Furthermore, fluid leakage into the 3D matrix surrounding the fracture results in proppant accumulation towards the saturation concentration in the lower aperture areas at the fracture bottom. This accumulation leads to significantly higher density and viscosity in these locations (Figure 8 bottom). Conversely, in the upper parts of the fracture, continuous settling prevents proppant particles from reaching the upper fracture boundaries. Consequently, this leads to diminishing proppant concentrations closer to the pure carrying fluid in the upper sections (Figure 8 middle). The presented model does not incorporate information about proppant particle size; however, a minimum aperture is required to enhance numerical convergence in the non-stimulated areas, resulting in a slight concentration of proppant below the stimulated areas. Introducing particle size information, typically in the order around a millimeter, would prevent proppant infiltration into the minimum aperture areas as well as the foremost areas of the fracture tip.

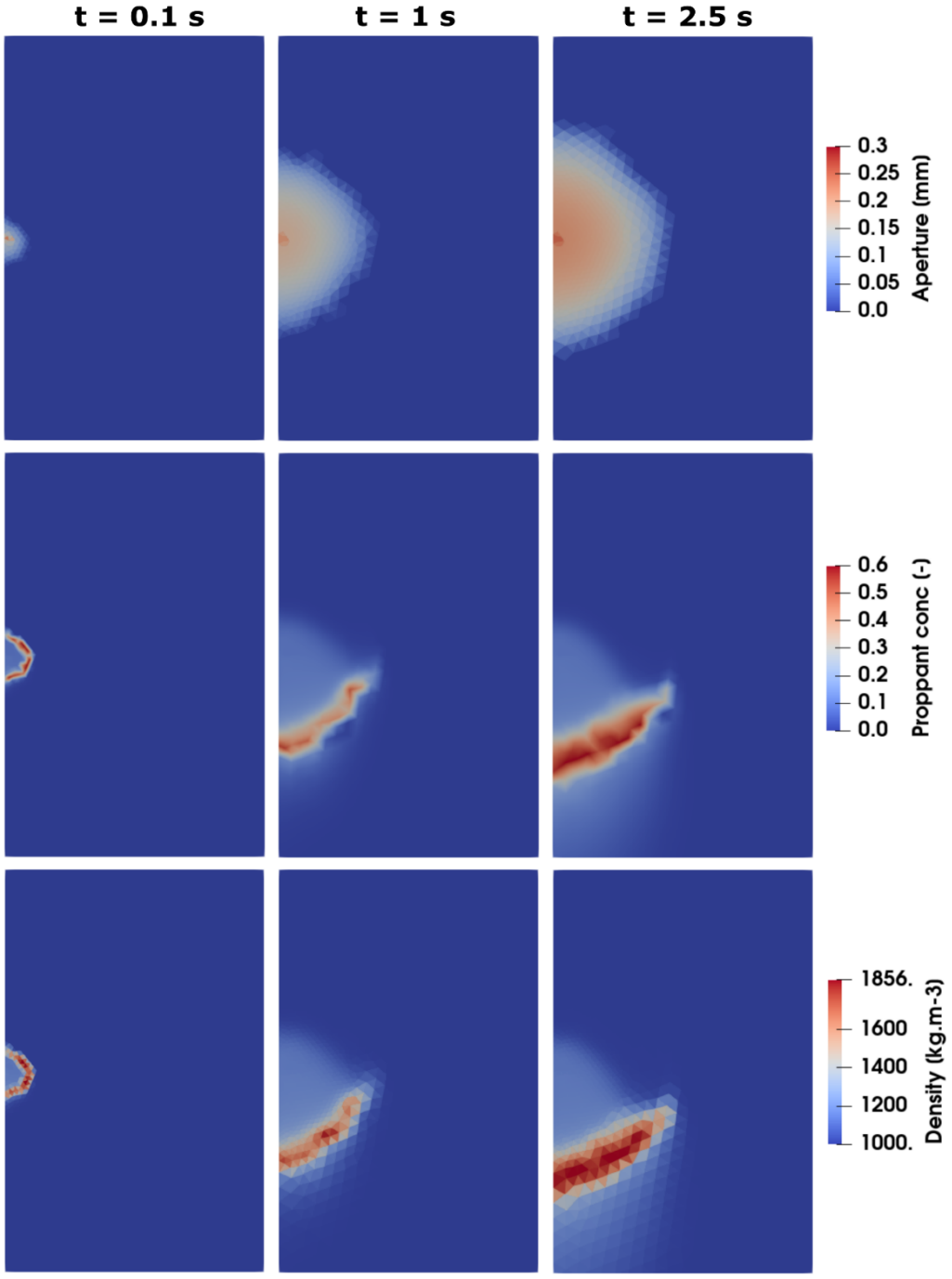

Figure 8: Aperture, proppant concentration and resulting slurry density distribution along the fracture plane.

4. CONCLUSION

We have developed a workflow to simulate the transport of proppant particles during hydraulic fracturing. This study primarily focuses on two workflows validating the transport of a particle-laden slurry and hydraulic fracturing in low-permeable host rock. The slurry comprises a mixture of low-viscosity fracturing fluid and high-density proppant particles. The processes involved include advective slurry transport, settling on the bottom of the fracture, and hindered settling due to particle-particle interactions. For simulating hydraulic fracturing, we utilize a novel CZM scheme, which efficiently simulates continuous fluid injection into a penny-shaped fracture geometry.

Both workflows were originally developed in the multiphysical MOOSE framework. The proppant transport code (ELK) is benchmarked against experimental and numerical results (Egert et al. 2023). The hydraulic fracturing code (KitFox) is extended to simulate continuous injection into a penny-shaped fracture geometry (Liu et al. 2024). The numerical simulation is successfully compared and benchmarked against the analytical solution of a toughness-storage dominated hydraulic fracture (Dontsov 2016). Preliminary results demonstrate the extension of the penny-shaped fracture model to include simultaneously injected slurry instead of pure water, loosely coupled using a MultiApp approach. We successfully show the flow of the particle-laden slurry into the propagating fracture. Initially, the high internal pressure gradient drives radial propagation of the proppant along with the fracture tip. As injection time and fracture length increase, gravitational settling becomes the dominant process, causing the proppant to preferentially accumulate at the bottom of the fracture, causing increasing pressure, density, and viscosity. Consequently, proppant-depleted carrying fluid exists at the top of the fracture. Further work will involve considering particle size as a limiting factor for proppant propagation into the small-aperture fracture tip. Additionally, we plan to incorporate back-coupling of further parameters into the hydraulic fracturing code. The proppant code will also be extended to consider pressure release, fracture closure, and trapped proppant to simulate field-scale hydraulic fracturing. These enhancements will enable a more comprehensive and realistic modeling of hydraulic fracturing processes at larger scales.

ACKNOWLEDGEMENT

The information, data, or work presented herein was funded in part by the Advanced Research Projects Agency-Energy (ARPA-E), U.S. Department of Energy (DOE), under Award Number DE-AR0001709. Any opinions, findings and conclusions, or recommendations expressed in this material are those of the authors and do not necessarily reflect those of the DOE or the U.S. Government. This research made use of Idaho National Laboratory computing resources, which are supported by the Office of Nuclear Energy of the U.S. DOE and the Nuclear Science User Facilities under Contract No. DE-AC07-05ID14517. This work is partially supported through the Idaho National Laboratory Laboratory Directed Research & Development (LDRD) Program under the U.S. Department of Energy Idaho Operations Office Contract DE-AC07-05ID14517.

REFERENCES

Adachi, J., Siebrits, E., Peirce, A. and Desroches, J.: Computer simulation of hydraulic fractures, International Journal of Rock Mechanics and Mining Sciences, 44, 5, (2007), 739-757.

Aslannezhad, M., Kalantariasl, A., You, Z., Iglauer, S. and Keshavarz, A.: Micro-proppant placement in hydraulic and natural fracture stimulation in unconventional reservoirs: A review, Energy Reports, 7, (2021), 8997-9022.

Barboza, B. R., Chen, B. and Li, C.: A review on proppant transport modelling, Journal of Petroleum Science and Engineering, 204, (2021).

Chen, B., Barboza, B. R., Sun, Y., Bai, J., Thomas, H. R., Dutko, M., Cottrell, M. and Li, C.: A Review of Hydraulic Fracturing Simulation, Archives of Computational Methods in Engineering, 29, 4, (2021), 1-58.

Chun, T., Li, Y. and Wu, K.: Comprehensive experimental study of proppant transport in an inclined fracture, Journal of Petroleum Science and Engineering, 184, (2020).

Costa, A., Hu, T. and Dolbow, J. E.: On formulations for modeling pressurized cracks within phase-field methods for fracture, Theoretical and Applied Fracture Mechanics, 127, (2023).

Detournay, E.: Mechanics of Hydraulic Fractures, Annual Review of Fluid Mechanics, 48, 1, (2016), 311-339.

Dontsov, E. V.: An approximate solution for a penny-shaped hydraulic fracture that accounts for fracture toughness, fluid viscosity and leak-off, R Soc Open Sci, 3, 12, (2016), 160737.

Egert, R., Gholami Korzani, M., Held, S. and Kohl, T.: Thermo-hydraulic Modeling of an Enhanced Geothermal System in the Upper Rhine Graben using MOOSE/TIGER, Proceedings WGC2020+1, Reykjavik, (2021).

Egert, R., Meng, C., Fournier, A. and Jin, W.: Numerical Study of Proppant Transport and Settling Processes in Fractures, GRC Transactions, 47, (2023), 545-558.

Egert, R., Nitschke, F., Gholami Korzani, M. and Kohl, T.: Stochastic 3D Navier-Stokes Flow in Self-Affine Fracture Geometries Controlled by Anisotropy and Channeling, Geophysical Research Letters, 48, 9, (2021).

Gaston, D. R., Permann, C. J., Peterson, J. W., Slaughter, A. E., Andrš, D., Wang, Y., Short, M. P., Perez, D. M., Tonks, M. R., Ortensi, J., Zou, L. and Martineau, R. C.: Physics-based multiscale coupling for full core nuclear reactor simulation, Annals of Nuclear Energy, 84, (2015), 45-54.

Geertsma, J. and De Klerk, F.: A Rapid Method of Predicting Width and Extent of Hydraulically Induced Fractures, Journal of Petroleum Technology, 21, 12, (1969), 1571-1581.

Hosseini, N. and Khoei, A. R.: Numerical simulation of proppant transport and tip screen-out in hydraulic fracturing with the extended finite element method, International Journal of Rock Mechanics and Mining Sciences, 128, (2020).

Huang, J., Hao, Y., Settgast, R. R., White, J. A., Mateen, K. and Gross, H.: Validation and Application of a Three-Dimensional Model for Simulating Proppant Transport and Fracture Conductivity, Rock Mechanics and Rock Engineering, (2022).

Isah, A., Hiba, M., Al-Azani, K., Aljawad, M. S. and Mahmoud, M.: A comprehensive review of proppant transport in fractured reservoirs: Experimental, numerical, and field aspects, Journal of Natural Gas Science and Engineering, 88, (2021).

Jia, Y., Tsang, C.-F., Hammar, A. and Niemi, A.: Hydraulic stimulation strategies in enhanced geothermal systems (EGS): a review, Geomechanics and Geophysics for Geo-Energy and Geo-Resources, 8, 6, (2022).

Jin, W. and Arson, C.: Fluid-driven transition from damage to fracture in anisotropic porous media: a multi-scale XFEM approach, Acta Geotechnica, 15, 1, (2019), 113-144.

Kumar, D., Gonzales, R. and Ghassemi, A.: The Role of Micro-Proppants in Conductive Fracture Network Development, SPE Hydraulic Fracturing Technology Conference and Exhibition, The Woodlands, (2019).

Lindsay, A. D., Gaston, D. R., Permann, C. J., Miller, J. M., Andrs, D., Slaughter, A. E., Kong, F. D., Hansel, J., Carlsen, R. W., Icenhour, C., Harbour, L., Giudicelli, G. L., Stogner, R. H., German, P., Badger, J., Biswas, S., Chapuis, L., Green, C. P., Hales, J., Hu, T. C., Jiang, W., Jung, Y. S., Matthews, C., Miao, Y. B., Novak, A., Peterson, J. W., Prince, Z. M., Rovinelli, A., Schunert, S., Schwen, D., Spencer, B. W., Veeraraghavan, S., Recuero, A., Yushu, D., Wang, Y. Q., Wilkins, A. and Wong, C. S. P.: 2.0-MOOSE: Enabling massively parallel multiphysics simulation, Softwarex, 20, (2022).

Liu, R., Jin, W., Harbour, L., Kong, F., Permann, C. J., Gaston, D. R. and Podgorney, R.: A robust interface finite element formulation for modeling brittle material failure problems, International Journal for Numerical Methods in Engineering, 124, 23, (2023), 5356-5374.

Liu, R., Permann, C. J., Gaston, D. R., Schwen, D., Wen, J., Hu, T., Jin, W. and Podgorney, R.: A Robust and Efficient Lower Dimensional Finite Element Method for Hydraulic Fracturing, Submitted, (2024).

Meng, C., Fournier, A. and Jin, W.: A Split-node Method for Modeling Pulse and Hydraulic Fracturing, ARMA Symposium, Atlanta, (2023).

Nordgren, R. P.: Propagation of a Vertical Hydraulic Fracture, Society of Petroleum Engineers Journal, 12, 04, (1972), 306-314.

Parker, R. H. and Jupe, A.: In situ leach mining and hot dry rock (HDR) geothermal energy technology, Minerals Engineering, 10, 3, (1997), 301-308.

Perkins, T. K. and Kern, L. R.: Widths of Hydraulic Fractures, Journal of Petroleum Technology, 13, 09, (1961), 937-949.

Shiozawa, S. and McClure, M.: Simulation of proppant transport with gravitational settling and fracture closure in a three-dimensional hydraulic fracturing simulator, Journal of Petroleum Science and Engineering, 138, (2016), 298-314.

Wang, J.: Propagation, proppant transport, and the evolution of transport properties of fluid-driven fractures, PhD, Pennsylvania State University, (2020).

Wilkins, A., Green, C. P. and Ennis-King, J.: An open-source multiphysics simulation code for coupled problems in porous media, Computers & Geosciences, 154, (2021).

Witherspoon, P. A., Wang, J. S. Y., Iwai, K. and Gale, J. E.: Validity of Cubic Law for fluid flow in a deformable rock fracture, Water Resources Research, 16, 6, (1980), 1016-1024.

Yao, S., Chang, C., Hai, K., Huang, H. and Li, H.: A review of experimental studies on the proppant settling in hydraulic fractures, Journal of Petroleum Science and Engineering, 208, (2022).

Zeng, J., Li, H. and Zhang, D.: Numerical simulation of proppant transport in propagating fractures with the multi-phase particle-in-cell method, Fuel, 245, (2019), 316-335.

Zhang, X., Wu, B., Yang, D. and Bunger, A.: Mechanics of Hydraulic Fracturing: Experiment, Model, and Monitoring, Wiley, (2022).